



# Analysis of static and dynamic characteristics of Secant slider bearing with MHD and couple stress fluid

B. N. Hanumagowda<sup>1</sup>, Tesymol Cyriac<sup>2</sup>, H.S. Doreswamy<sup>3</sup> and A. Salma<sup>4</sup>

## Abstract

Effects of couple stress and Magneto-hydrodynamics on a secant slider bearing are discussed in the present study. The basis of this discussion is the theory of couple stresses introduced by Stokes. Basic equations of motion are solved to derive pressure generated in the fluid and load carrying capacity of the bearing. Dynamic characteristics like damping coefficient and dynamic stiffness are also derived. Dynamic characteristics and the bearing performance, when squeezing is nil are evaluated by assigning some numerical values to the parameters. These results are illustrated graphically. It is concluded that the bearing characteristics, both steady and dynamic, will show an increasing trend in its values, when magnetic field is applied to the bearing structure and when fluids having couple stress are used to lubricate it.

## Keywords

Slider bearing, Couple stress, Magneto-hydrodynamics.

## AMS Subject Classification

37D08, 74DXX, 76E25.

<sup>1,4</sup> School of Applied Sciences, REVA University, Bengaluru, Karnataka, India.

<sup>2</sup> Muthoot Institute of Technology and Science, Ernalulam-682308, India.

<sup>2,3</sup> East Point College of Engineering and Technology, Bengaluru, Karnataka, India.

\*Corresponding author: hanumagowda123@rediffmail.com

Article History: Received 10 February 2020; Accepted 18 April 2020

©2020 MJM.

## Contents

1	Introduction .....	581
2	Mathematical Formulation .....	582
3	Results and Discussion .....	584
3.1	Dimensionless steady-state film pressure . . .	584
3.2	Dimensionless steady-state load carrying Capacity	585
3.3	Dynamic Stiffness . . . . .	585
3.4	Damping Coefficient . . . . .	585
4	Conclusion .....	586
	References .....	586

## 1. Introduction

Bearings are unavoidable elements of a machine that help different parts to move with respect to each other. The application area of each type of bearing is different. Hence design engineers must know about various types of bearings, their

applications and limitations. A thorough knowledge about the behavior of different bearing geometries under different operating conditions is essential for a design engineer. The dynamic characteristics represent the stability of moving part while the steady state performance assumes importance in the design phase of bearings.

Magneto-hydrodynamic bearings have been an active area of research for many years. Elco and Hughes [1] have done research on the properties of infinite inclined slider bearings with an applied magnetic field. They observed that application of electric and magnetic fields can increase the pressure built in the fluid film, when there is a supply of electrical energy to the bearing from an external source. Researchers such as Shukla [2], Kuzma [3] and Hazma [4] studied the effect of MHD on different bearing systems. All of them found that MHD enhances the bearing characteristics.

In practical applications, different lubrication mechanisms are used as per different requirements and applications to minimize friction and wear of bearings. It is known that interactions between microscopic elements which are present

in a complex fluid like liquid metals are the reason for classical Cauchy stresses and couple stresses in it.

There are many theories that describe polar effects in the lubricant. But, couple stress theory explained by Stokes [5] is the basic one among them, based on which diverse authors discussed the effect of couple stress on the performance characteristics of bearing element. Ramanaiah and Sarkar [6] conducted an analytical study on the effect of incompressible fluid, in which couple stresses are present, as the lubricant for infinitely long slider bearings. Bujurke and Jayaraman [7] carried out a theoretical study on non-Newtonian flow effects in squeeze film. They concluded that the presence of couple stress in the lubricant gives significant load carrying capacity and increases bearing life. In this, they referred synovial joints and synovial fluids as an example for the above said mechanism.

A theoretical analysis of slider bearings which are exposed to uniform magnetic field was conducted by Das [8]. The fluid he considered was incompressible, electrically conducting and isothermal couple stress fluid. His work proved supremacy of couple stress and magnetic parameters over Newtonian and non-magnetic fluids in increasing load carrying capacity. Further, we can understand that the shape of bearings also affect the values of maximum load capacity. The effects of couple stress fluids on the performance of finite journal bearings was studied by Lin [9] and he observed that the lubrication features like load carrying capacity and friction parameters are improved in the presence of couple stress. Characteristics of two-lobe journal bearings coated with couple-stress fluids are studied by Crosby and Chetti [10] and they concluded that the presence of couple stress influences the performance of journal bearing significantly. It is also seen that stability is more when the bearings are lubricated with non-Newtonian fluid instead of Newtonian fluids.

The impact of magnetohydrodynamics and couple stress on porous composite slider bearing was investigated by Bidadar and Hanumagowda [11]. Results were discussed for different values of permeability parameter in it. Hanumagowda [12] studied the effect of magnetohydrodynamics and couple stress on the characteristics of plane slider bearing and concluded that because of it, the characteristics of plane slider bearing, both steady and dynamic, are improved. Bujurke and Naduvinamani [13], Fathima *et.al* [14] and several researchers [15]-[18] analyzed the effect of couple stress and MHD in various aspects.

All these research works showed that, the presence of couple stress has a notable role on the working of a bearing system as compared to Newtonian case. In the present paper, the influence of couple stress and MHD on a secant slider bearing is analyzed.

## 2. Mathematical Formulation

The geometrical structure of a secant slider bearing is presented in Figure 1. A magnetic field is applied to it in the perpendicular direction.

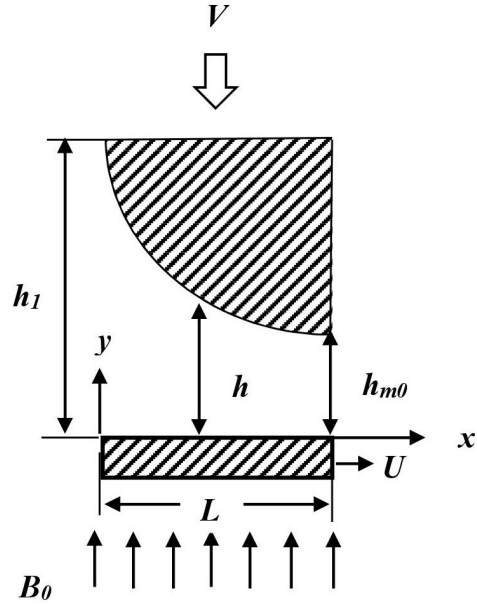


Figure 1: Schematic diagram of secant slider bearing.

Basic Equations of motion are:

$$\frac{\partial u}{\partial x} + \frac{\partial v}{\partial y} = 0 \tag{2.1}$$

$$\mu \frac{\partial^2 u}{\partial y^2} - \eta \frac{\partial^4 u}{\partial y^4} - \sigma B_0^2 u = \frac{\partial p}{\partial x} + \sigma E_z B_0 \tag{2.2}$$

$$\frac{\partial p}{\partial y} = 0 \tag{2.3}$$

$$\int_{y=0}^h (E_z + B_0 u) dy = 0 \tag{2.4}$$

The film thickness of the secant slider bearing can be taken as

$$h(x, t) = h_m(t) \sec(a(1-x)) \tag{2.5}$$

$$a = \sec^{-1}(\delta + 1) \tag{2.6}$$

$$\delta = \frac{h_1 - h_{m0}}{h_{m0}} \tag{2.7}$$

$h_{m0}(t)$  is the minimum film thickness.

For the problem being discussed, the following boundary conditions are assumed.

At the upper surface we have  $y = h$

$$u = 0, \quad \frac{\partial^2 u}{\partial y^2} = 0, \quad v = -\frac{\partial h}{\partial t} = -V \tag{2.8}$$

At the lower surface we have  $y = 0$

$$u = U, \quad \frac{\partial^2 u}{\partial y^2} = 0, \quad v = 0 \tag{2.9}$$

Solution of Equation (2.2) and (2.4) after applying the above boundary conditions (2.8) and (2.9) is

$$u = -\frac{U}{2} v_1 - \frac{h_{m0}^2 h}{2l\mu M_0^2} \frac{\partial p}{\partial x} v_2 \tag{2.10}$$



where

$$v_1 = v_{11} - v_{12}, v_2 = v_{13} - v_{14}, \text{ for } 4M_0^2 l^2 / h_{m0}^2 < 1 \quad (2.11)$$

$$v_1 = v_{21} - v_{22}, v_2 = v_{23} - v_{24}, \text{ for } 4M_0^2 l^2 / h_{m0}^2 = 1 \quad (2.12)$$

$$v_1 = v_{31} - v_{32}, v_2 = v_{33} - v_{34}, \text{ for } 4M_0^2 l^2 / h_{m0}^2 > 1 \quad (2.13)$$

where  $l = (\frac{\eta}{\mu})^{\frac{1}{2}}$  is the couple stress parameter,  $M_0 = B_0 h_{m0} (\frac{\sigma}{\mu})^{\frac{1}{2}}$  is the Hartmann number and  $h_{m0}$  is minimum film thickness.

Expressions for  $v_1$  and  $v_2$  in the three different cases as specified by the conditions in the equation set (2.11), (2.12), (2.13) are provided in the Appendix I.

Modified Reynolds's equation can be derived by integrating (2.1) and applying boundary conditions given by (2.8) and (2.9). In case of secant slider bearing, it is found to be

$$\frac{\partial}{\partial x} \left\{ f(h, l, M_0) \frac{\partial p}{\partial x} \right\} = 6U \frac{\partial h}{\partial x} + 12 \frac{\partial h}{\partial t} \quad (2.14)$$

Where,

$$f(h, l, M_0) = \begin{cases} \frac{6h_{m0}^2 h^2}{\mu l M_0^2} \left\{ \frac{A^2 - B^2}{B \tanh \frac{Bh}{2l} - \frac{B^2 \tanh \frac{Ah}{2l}}{A}} - \frac{2l}{h} \right\} & \text{for } 4M_0^2 l^2 / h_{m0}^2 < 1, \\ \frac{6h_{m0}^2 h^2}{\mu l M_0^2} \left\{ \frac{2(\cosh(h/\sqrt{2}l) + 1)}{3\sqrt{2} \sinh(h/\sqrt{2}l) - h/l} - \frac{2l}{h} \right\} & \text{for } 4M_0^2 l^2 / h_{m0}^2 = 1, \\ \frac{6h_{m0}^2 h^2}{\mu l M_0^2} \left\{ \frac{2M_0(\cos B_1 h + \cosh A_1 h)}{h_2(A_2 \sin B_1 h + B_2 \sinh A_1 h)} - \frac{2l}{h} \right\} & \text{for } 4M_0^2 l^2 / h_{m0}^2 > 1, \end{cases} \quad (2.15)$$

Equation (2.14) can be converted to its non – dimensional form by using the following relations.

$$x^* = \frac{x}{L}, t^* = \frac{Ut}{L}, P^* = \frac{ph_{m0}^2}{\mu UL}, I^* = \frac{2l}{h_{m0}}, M_0 = B_0 h_{m0} \left(\frac{\sigma}{\mu}\right)^{1/2}, h^*(x^*, t^*) = \frac{h}{h_{m0}} \quad (2.16)$$

Substituting above values in (2.14) and (2.15), the modified Reynolds's equation takes the following non- dimensional form.

$$\frac{\partial}{\partial x^*} \left\{ f(h^*, I^*, M_0) \frac{\partial P^*}{\partial x^*} \right\} = 6h_m^*(t^*) \frac{\partial(\sec(a(1-x^*)))}{\partial x^*} + 12 \sec(a(1-x^*)) V^* \quad (2.17)$$

Where,  $h^*(x, t) = h_m^*(t^*) \sec(a(1-x^*))$ ,  $V^* = \frac{dh_m^*}{dt^*}$

$$f(h^*, I^*, M_0) = \begin{cases} \frac{12h^{*2}}{I^{*2} M_0^2} \left\{ \frac{A^{*2} - B^{*2}}{B^* \tanh \frac{B^* h^*}{I^*} - \frac{B^{*2} \tanh \frac{A^* h^*}{I^*}}{A^*}} - \frac{I^*}{h^*} \right\} & \text{for } M_0^2 I^{*2} < 1, \\ \frac{12h^{*2}}{I^{*2} M_0^2} \left\{ \frac{1 + \cosh(\sqrt{2}h^*/I^*)}{(3\sqrt{2}) \sinh(\sqrt{2}h^*/I^*) - h^*/I^*} - \frac{I^*}{h^*} \right\} & \text{for } M_0^2 I^{*2} = 1, \\ \frac{12h^{*2}}{I^{*2} M_0^2} \left\{ \frac{M_0(\cos B_1^* h^* + \cosh A_1^* h^*)}{(A_2^* \sin B_1^* h^* + B_2^* \sinh A_1^* h^*)} - \frac{I^*}{h^*} \right\} & \text{for } M_0^2 I^{*2} > 1, \end{cases} \quad (2.18)$$

$$A^{*2} = \frac{1 + \sqrt{1 - I^{*2} M_0^*}}{2}, B^{*2} = \frac{1 - \sqrt{1 - I^{*2} M_0^*}}{2},$$

$$A_1^* = \sqrt{\frac{2M_0}{I^*}} \cos\left(\frac{\theta^*}{2}\right), B_1^* = \sqrt{\frac{2M_0}{I^*}} \sin\left(\frac{\theta^*}{2}\right),$$

$$A_2^* = (B_1^* - A_1^* \cot \theta^*), B_2^* = (A_1^* + B_1^* \cot \theta^*),$$

$$\theta^* = \tan^{-1}(\sqrt{I^{*2} M_0^2 - 1})$$

Integrating (2.16) two times with respect to  $x^*$  and then applying the boundary conditions

$$P^* = 0 \text{ at } x^* = 0 \text{ and } x^* = 1$$

We get the film pressure as

$$P^* = 6h_m^*(t^*) J_1(0, x^*) - \frac{12V^*}{a} J_2(0, x^*) + \left\{ - \frac{6h_m^*(t^*) J_1(0, x^*) - \frac{12V^*}{a} J_2(0, x^*)}{J_3(0, 1)} \right\} J_3(0, x^*), \quad (2.19)$$

where

$$J_1(0, x^*) = \int_{x^*=0}^{x^*} \frac{\sec(a(1-x^*))}{f^*(h^*, I^*, M_0)} dx^*, J_1(0, 1) = \int_{x^*=0}^1 \frac{\sec(a(1-x^*))}{f^*(h^*, I^*, M_0)} dx^*,$$

$$J_2(0, x^*) = \int_{x^*=0}^{x^*} \frac{\ln[\sec(a(1-x^*)) + \tan(a(1-x^*))]}{f^*(h^*, I^*, M_0)} dx^*,$$

$$J_2(0, 1) = \int_{x^*=0}^1 \frac{\ln[\sec(a(1-x^*)) + \tan(a(1-x^*))]}{f^*(h^*, I^*, M_0)} dx^*,$$

$$J_3(0, x^*) = \int_{x^*=0}^{x^*} \frac{1}{f^*(h^*, I^*, M_0)} dx^*, J_3(0, 1) = \int_{x^*=0}^1 \frac{1}{f^*(h^*, I^*, M_0)} dx^*.$$

The load applied over a length of  $L$  is given by

$$w = \int_0^L p dx.$$

Load carrying capacity in terms of non-dimensional quantity is given by,

$$W^* = \int_{x^*=0}^1 P^* dx^*$$

$$W^* = 6h_m^*(t^*) \int_0^1 J_1(0, x^*) dx^* - \frac{12V^*}{a} \int_0^1 J_2(0, x^*) dx^*$$

$$+ \left\{ - \frac{6h_m^*(t^*) J_1(0, x^*) dx^* - \frac{12V^*}{a} J_2(0, 1)}{J_3(0, 1)} \right\} \int_0^1 J_3(0, x^*) dx^* \quad (2.20)$$

For the next steps, assuming minimum film height as a constant and considering squeezing velocity as nil, the dimensionless steady state pressure  $P_s^*$  and load carrying capacity  $W_s^*$  take the following form.

$$P_s^* = 6h_m^*(t^*) J_1(0, x^*) - \frac{6h_m^*(t^*) J_1(0, 1)}{J_3(0, 1)} J_3(0, x^*) \quad (2.21)$$

$$W_s^* = 6h_m^*(t^*) \int_0^1 J_1(0, x^*) dx^* - \frac{6h_m^*(t^*) J_1(0, 1)}{J_3(0, 1)} \int_0^1 J_3(0, x^*) dx^* \quad (2.22)$$

Dynamic stiffness coefficient is given by

$$S_d^* = - \left( \frac{\partial W_s^*}{\partial h_m^*} \right) \quad (2.23)$$

Dynamic damping coefficient is given by

$$D_d^* = - \left( \frac{\partial W^*}{\partial V^*} \right) \quad (2.24)$$



### 3. Results and Discussion

This paper presents a comparison of secant slider bearing performance, when lubricated with Newtonian and non – Newtonian fluids in the presence/absence of magnetic field. Apart from this, changes in dynamic characteristics of secant slider bearing, when lubricated with couple stress fluid in the presence of magnetic field, is analyzed. It is observed that the behavior of the secant slider bearing is better in the presence of magnetic field. It is also seen that, bearing characteristics improve with the presence of couple stress in the fluid. Results are illustrated below for some particular values of  $M_0$ ,  $l^*$  and  $h_m^*$ .

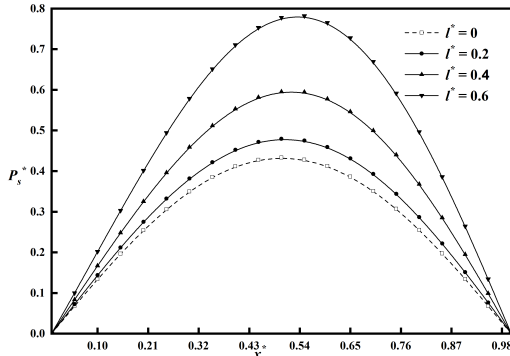


Figure 2: Plot of steady film pressure  $P_s^*$  against  $x^*$  for different values of  $l^*$  with  $M_0=3$  and  $\delta=0.8$  and  $h_m^*=0.8$

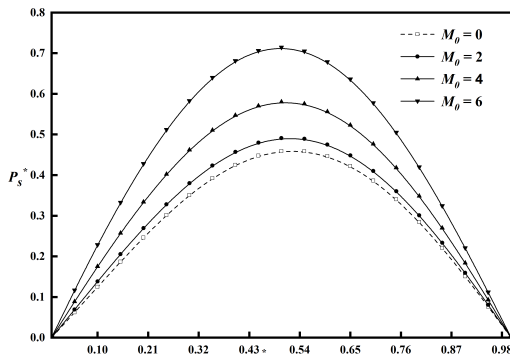


Figure 3: Plot of steady film pressure  $P_s^*$  against  $x^*$  for different values of  $M_0$  with  $l^*=0.3$  and  $\delta=0.8$  and  $h_m^*=0.8$

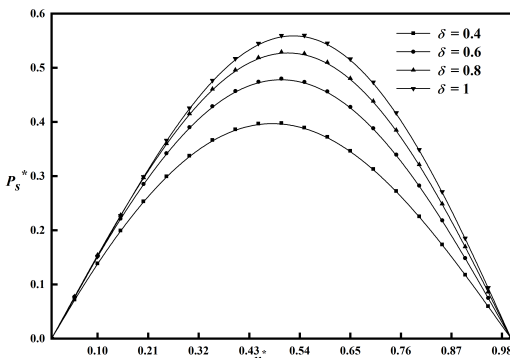


Figure 4: Plot of steady film pressure  $P_s^*$  against  $x^*$  for different values of  $\delta$  with  $M_0=3$  and  $l^*=0.3$  and  $h_m^*=0.8$

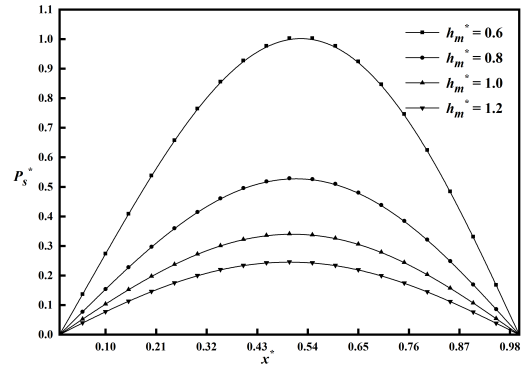


Figure 5: Plot of steady film pressure  $P_s^*$  against  $x^*$  for different values of  $h_m^*$  with  $M_0=3$ ,  $l^*=0.3$  and  $\delta=0.8$ .

#### 3.1 Dimensionless steady-state film pressure

The variation of  $P_s^*$  against  $x^*$  for certain values of  $l^*$  by taking  $M_0=3$ ,  $\delta=0.8$  and  $h_m^*=0.8$  is shown in Figure2. From the graph, it is clear that as the value of  $l^*$  increases, the value of  $P_s^*$  also increases. The steady film pressure  $P_s^*$  against  $x^*$  for certain values of  $M_0$  is plotted in Figure3. In the same plot, it can be seen that, the steady film pressure shows increasing trend as the magnetic field is increased. Figure4 is the plot of  $P_s^*$  against  $x^*$  for different values of  $\delta$  by taking  $M_0=3$ ,  $l^*=0.3$  and  $h_m^*=0.8$ . One can observe that  $P_s^*$  increases as  $\delta$  increases. Further, Figure5, shows a drop in dimensionless steady film pressure for increasing minimum film height,  $h_m^*$ .

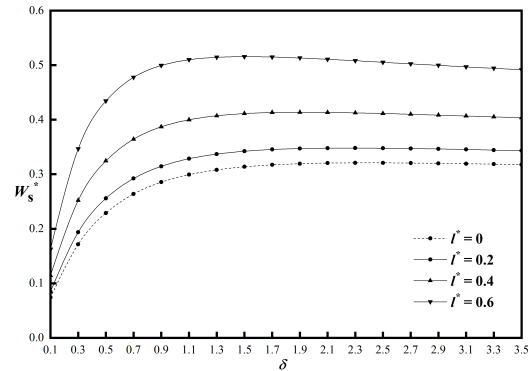


Figure 6: Plot of steady load carrying capacity  $W_s^*$  against  $\delta$  for different values of  $l^*$  with  $M_0=3$  and  $h_m^*=0.8$ .

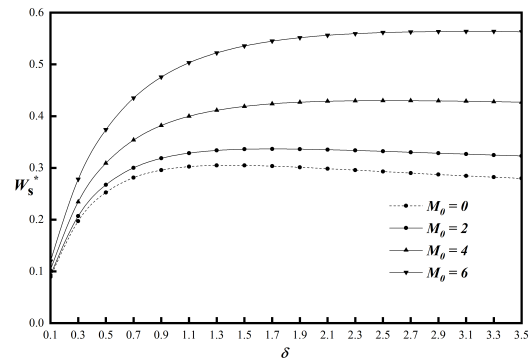


Figure 7: Plot of steady load carrying capacity  $W_s^*$  against  $\delta$  for different values of  $M_0$  with  $l^*=0.3$  and  $h_m^*=0.8$ .



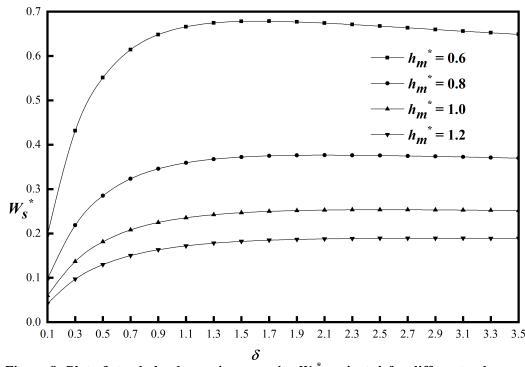


Figure 8: Plot of steady load carrying capacity  $W_s^*$  against  $\delta$  for different values of  $h_m^*$  with  $l^* = 0.3$  and  $M_0 = 3$ .

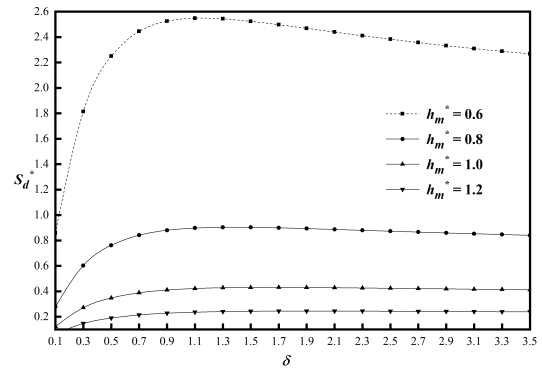


Figure 11: Plot of Dynamic Stiffness  $S_d^*$  against  $\delta$  for different values of  $h_m^*$  with  $M_0 = 3$  and  $l^* = 0.3$ .

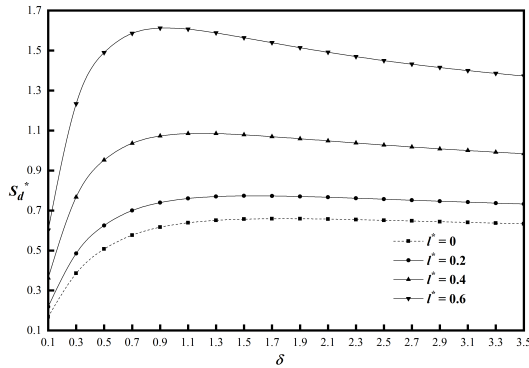


Figure 9: Plot of Dynamic Stiffness  $S_d^*$  against  $\delta$  for different values of  $l^*$  with  $M_0 = 3$  and  $h_m^* = 0.8$ .

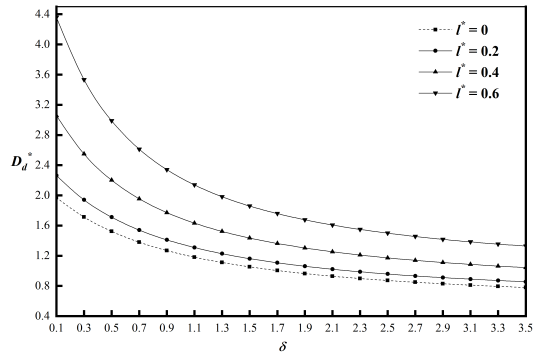


Figure 12: Plot of Damping coefficient  $D_d^*$  against  $\delta$  for different values of  $l^*$  with  $M_0 = 3$  and  $h_m^* = 0.8$ .

### 3.2 Dimensionless steady-state load carrying Capacity

Figure 6- Figure 8 illustrate the variation of  $W_s^*$  against  $\delta$ . Figure 6 clearly shows that steady load carrying capacity is more for a non-Newtonian fluid than a Newtonian one. Also it increases with  $l^*$ . Figure 7 shows the improvement of steady load carrying capacity with the application of magnetic field. Figure 8 demonstrates the change in the load carrying capacity when the minimum value of film height increases. With symbols we can write, when  $h_m^*$  increases,  $W_s^*$  decreases.

### 3.3 Dynamic Stiffness

Variation of dynamic stiffness  $S_d^*$  against  $\delta$  in different cases are shown in figures 9, 10 and 11. Figure 9 shows change in the values

of dynamic stiffness as couple stress parameter takes different values when  $M_0 = 3$  and  $h_m^* = 0.8$ . It is obvious that the couple stress parameter enhances the dynamic stiffness. Figure 10 explains the effect of magnetic field on dynamic stiffness. As the Hartmann number  $M_0$  increases, dynamic stiffness also increases. Figure 11 clearly tells the effect of small value of film thickness on the dynamic stiffness. The stiffness is more when the film thickness is less.

### 3.4 Damping Coefficient

Variation of  $D_d^*$  against  $\delta$  in different cases are shown in figures 12, 13 and 14. In all these graphs,  $D_d^*$  decreases as  $\delta$  increases. From Figure 12, it is observed that damping coefficient increases as couple stress parameter increases. Figure 13 shows that the damping

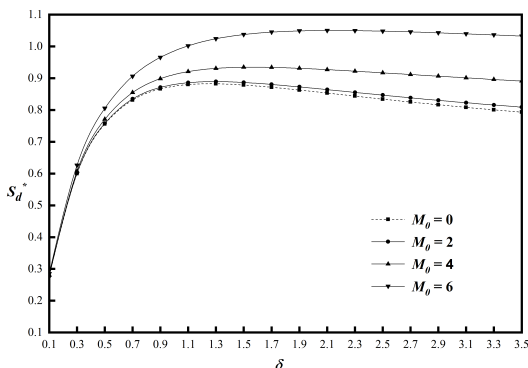


Figure 10: Plot of Dynamic Stiffness  $S_d^*$  against  $\delta$  for different values of  $M_0$  with  $l^* = 0.3$  and  $h_m^* = 0.8$ .

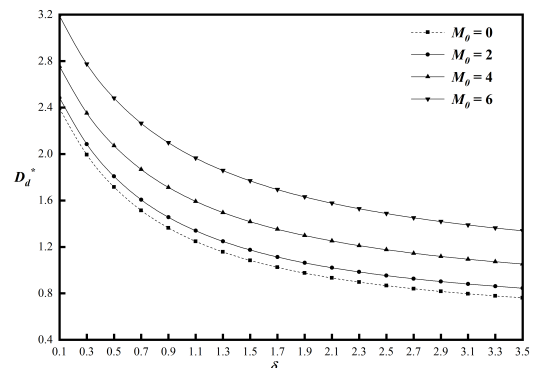


Figure 13: Plot of Damping coefficient  $D_d^*$  against  $\delta$  for different values of  $M_0$  with  $l^* = 0.3$  and  $h_m^* = 0.8$ .



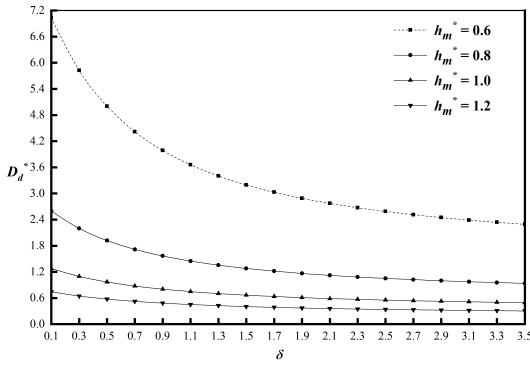


Figure 14: Plot of Damping coefficient  $D_d^*$  against  $\delta$  for different values of  $h_m^*$  with  $M_0 = 3$  and  $l' = 0.3$

coefficient increases as  $M_0$  increases. Figure 14 shows the variation of  $D_d^*$  for certain values of minimum film thickness,  $h_m^*$ . One can make out that the damping coefficient drops in value with an increasing  $h_m^*$ .

## 4. Conclusion

On the basis of Stoke's theory on micro continuum fluid, static and dynamic characteristics of secant slider bearing when the fluid is subjected to magnetic field and couple stress is analyzed. From the results, it can be arrived at the following conclusions.

1. All four characteristics under study, namely, steady-state film pressure, steady-state load carrying capacity, damping coefficient and dynamic stiffness for a secant slider bearing shows an increase as the Hartmann number  $M_0$  increases. The performance of the bearing is found to be better in magnetic case (when  $M_0 > 0$ ) compared to non-magnetic case (when  $M_0$  is 0).
2. The steady-state film pressure, steady-state film load carrying capacity, damping coefficient and dynamic stiffness of the secant slider bearing, increase with the increase in the couple stress parameter. The performance is found to be better when non-Newtonian fluid is used as lubricant compared to Newtonian Fluid.
3. The steady-state film pressure, steady-state load carrying capacity, damping coefficient and dynamic stiffness of the secant slider bearing, decrease with increase in the minimum thickness of the fluid film.

## Appendix:I

$$V_{11} = \frac{B^2}{(A^2 - B^2)} \left\{ \frac{\sinh(Ah/1) - \sinh(Ay/l) - \sinh(A(h-y)/l)}{\sinh(Ah/l)} \right\}$$

$$V_{12} = \frac{A^2}{(A^2 - B^2)} \left\{ \frac{\sinh(Bh/1) - \sinh(By/l) - \sinh(B(h-y)/l)}{\sinh(Bh/l)} \right\}$$

$$V_{13} = \frac{B^2 \{ \sinh(Ah/1) - \sinh(Ay/l) + \sinh(A(h-y)/l) \}}{\sinh(Ah/1) \{ (B^2/A) \tanh(Ah/21) - (A^2/B) \tanh(Bh/21) \}}$$

$$V_{14} = \frac{A^2 \{ \sinh(Bh/1) - \sinh(By/l) + \sinh(B(h-y)/l) \}}{\sinh(Bh/1) \{ (B^2/A) \tanh(Ah/21) - (A^2/B) \tanh(Bh/21) \}}$$

$$A = \left\{ \frac{1 + [1 - (4l^2 M_0^2 / h_0^2)]^{1/2}}{2} \right\}^{1/2}, B = \left\{ \frac{1 - [1 - (4l^2 M_0^2 / h_0^2)]^{1/2}}{2} \right\}^{1/2}$$

$$V_{21} = \frac{\sinh[(y-h)/\sqrt{2}l] + \sinh(y/\sqrt{2}l) - \sinh(h/\sqrt{2}l)}{\sinh(h/\sqrt{2}l)}$$

$$V_{22} = \frac{y \cosh[(y-h)/\sqrt{2}l] + y \cosh(y/\sqrt{2}l) - h \coth(h/2\sqrt{2}l) \sinh(h/\sqrt{2}l)}{2\sqrt{2}l \sinh(h/\sqrt{2}l)}$$

$$V_{23} = \frac{y \sinh[(y-h)/\sqrt{2}l] + y \sinh(y/\sqrt{2}l) - h \sinh(y/\sqrt{2}l)}{6l \sinh(h/\sqrt{2}l) - \sqrt{2}h}$$

$$V_{24} = \frac{2 \cosh[(y-h)/\sqrt{2}l] + 2 \cosh(y/\sqrt{2}l) - 2 \cosh(h/\sqrt{2}l) - 2}{3\sqrt{2}l \sinh(h/\sqrt{2}l) - (h/l)}$$

$$V_{31} = \frac{\cosh(A_1 y) \cos(B_1(y-h)) - \cos(B_1 y) \cosh(A_1(y-h))}{\cosh(A_1 h) - \cos(B_1 h)}$$

$$V_{32} = \frac{\cot \theta \{ \sinh(A_1 y) \sin(B_1(y-h)) - \sin(B_1 y) \sinh(A_1(y-h)) \} + \cosh(A_1 h) - \cos(B_1 h)}{\cosh(A_1 h) - \cos(B_1 h)}$$

$$V_{33} = \frac{\cot \theta \{ \sinh(B_1 y) \sin(A_1(y-h)) + \sin(A_1 y) \sinh(B_1(y-h)) \} + \cos(B_1 h) + \cosh(A_1 h)}{(B_1 - A_1 \cot \theta) \sin(B_1 h) + (A_1 + B_1 \cot \theta) \sinh(A_1 h)}$$

$$V_{34} = \frac{\cos(B_1 y) \cosh(A_1(y-h)) + \cos(B_1(y-h)) \cosh(A_1 y)}{(B_1 - A_1 \cot \theta) \sin(B_1 h) + (A_1 + B_1 \cot \theta) \sinh(A_1 h)}$$

$$A_1 = \sqrt{M_0 / l h_0} \cos(\theta/2), B_1 = \sqrt{M_0 / l h_0} \sin(\theta/2), \theta = \tan^{-1}(\sqrt{4l^2 M_0^2 / h_0^2 - 1}).$$

## References

- [1] R. A. Elco and W. F. Hughes., Magnetohydrodynamic pressurization of liquid metal bearings, *Wear*, 5(1962), 198-212.
- [2] J. B. Shukla., The magnetohydrodynamic composite slider bearing, *Wear*, 7(1964), 460-465.
- [3] D.C. Kuzma., The magneto hydrodynamic parallel plate slider bearing, *Journal of Basic Engineering*, 87(3)(1965), 778-780.
- [4] E. A. Hazma., The magneto hydrodynamic squeeze film, *Journal of Tribology*, 110(2)(1986), 375-377.
- [5] V.K. Stokes., Couple Stresses in Fluids, *Physics of Fluids*, 9(9)(1966), 1709-1716.
- [6] G. Ramanaiah and P. Sarkar., Slider Bearings Lubricated by Fluids with Couple Stress, *Wear*, 52(1)(1979), 27-36.
- [7] N. M. Bujurke and G. Jayaraman., The influence of couple stresses in squeeze films, *International Journal of Mechanical Sciences*, 24(6)(1982), 369-376.
- [8] N. C. Das., A Study of Optimum Load Bearing Capacity for Slider Bearings Lubricated with Couple-Stress Fluids in Magnetic Field, *Tribology International*, 31(1998), 393-400.
- [9] J. R. Lin., Effects off couple stresses on the lubrication of finite journal bearings, *Wear*, 206(1997), 171-178.
- [10] W. A. Crosby and B. Chetti., The static and dynamic characteristics of a two-lobe journal bearing lubricated with couple-stress fluid, *Tribology Transactions*, 52(2)(2009), 262-268.



- [11] K. Biradar and B. N. Hanumangowda., MHD Effect on Porous Wide Composite Slider Bearings Lubricated with a Couple-stress Fluids, *Tribology Online*, 10(1)( 2015), 11-20.
- [12] B. N. Hanumangowda., Effect of Magnetohydrodynamics and Couple stress on Steady and dynamic characteristics of Plane Slider bearing, *Tribology Online*, 11(1)(2016), 40-49.
- [13] N. M. Bujurke and N. B. Naduvinamani., On the performance of narrow porous journal bearing lubricated with couple stress fluid, *Acta Mechanica*, 86(1)(1991), 179-191.
- [14] S. T. Fathima, N. B. Naduvinamani, B. N. Hanumagowda and J. S. Kumar., Modified Reynolds Equation for Different Types of Finite Plates with the Combined Effect of MHD and Couple Stresses, *Tribology Transactions*, 58(4)(2015), 660-667.
- [15] B. N. Hanumagowda, A. Siddangouda , C. S. Nagarajappa and J. Santhosh Kumar., Squeeze Film Lubrication Between Hydro-magnetic Porous Parallel Stepped Plates, *IOSR Journal of Engineering*, 08(6)(2018), 87-95.
- [16] Biradar Kashinath., Magneto hydrodynamic Couple stress Squeeze Film Lubrication of Triangular Plates, *International Journal of Engineering Inventions*, 3 (3)(2013), 66-73.
- [17] J. R. Lin, R. F. Lu and W. H. Liao., Analysis of magneto-hydrodynamic squeeze film characteristics between curved annular plates, *Industrial Lubrication and Tribology*, 56(5)(2004), 300-305.
- [18] J. R. Lin., Magneto-hydrodynamic squeeze film characteristics for finite rectangular plates, *Industrial Lubrication and Tribology*, 55(2)(2003), 84-89.

\*\*\*\*\*  
ISSN(P):2319 – 3786  
Malaya Journal of Matematik  
ISSN(O):2321 – 5666  
\*\*\*\*\*

